International Journal of Physics and Mathematics

E-ISSN: 2664-8644
P-ISSN: 2664-8636
IJPM 2023; 5(2): 63-69

www.physicsjournal.net
Received: 10-09-2023
Accepted: 12-10-2023

RP Singh
Department of Physics, S.S.V. College, Hapur, affiliated to C.C.S. University, Meerut, India

Corresponding Author:
RP Singh
Department of Physics, S.S.V. College, Hapur, affiliated to C.C.S. University, Meerut, India

Ab initio investigations of opto-electronic properties of ternary Tm-based thallium ditelluride

RP Singh

DOI: https://www.doi.org/10.33545/26648636.2023.v5.i2a.121

Abstract
The present research focuses on the electronic and optical properties of Tm-based thallium ditelluride ($TlTmTe_2$). Spin-polarized electronic structure calculations were performed using the PBE-GGA exchange-correlation functional. The electronic band structure reveals half-metallic nature of $TlTmTe_2$, characterized by a predominance of spin-down states at the Fermi level. Optical properties were also investigated using the same exchange correlation functional. The calculated values of the static dielectric function and refractive index were found consistent with the Penn model, thereby validate the optical results. The pronounced ultraviolet (UV) absorption behavior of $TlTmTe_2$ highlights its potential as a potential material for UV-sensitive applications such as photovoltaic devices, photodetectors, and UV shielding technologies.

Keywords: $TlTmT_2$; electronic; optical properties

Introduction
Half-metals are unique materials that conduct electrons of one spin orientation while blocking the other, combining metallic and semiconducting characteristics [1, 2]. Most are fully spin-polarized and exhibit ferromagnetism, making them suitable for spintronic applications such as spin valves, giant magneto-resistance, tunnelling magneto-resistance, and non-volatile magnetic random-access memory [3-5]. Semimetals offer high optical conductivity owing to high carrier mobility [6]. Thermodynamically, half-metals behave like metals but generally have lower thermal and electrical conductivity [7].
Thallium rare earth chalcogenides, are promising candidates for high-performance spintronic, thermoelectric and optoelectronic device applications, as they exhibit halfmetallic or semiconducting character. Here, $TlTmTe_2$, a Tm-based thallium ditelluride crystallizing in the α-$NaFeO_2$-type structure (space group R-3m) [8], has been investigated for its electronic and optical properties. Our results reveal that $TlTmTe_2$ is a half-metallic material, making it a strong candidate for future spintronics and optoelectronic applications.
Previous studies on related compounds, such as $TlRX_2$ (where, R= rare earth elements, and X = chalcogen elements *viz.* S, Se, Te) reported the promising thermoelectric and magnetic properties [8-14]. For instance, Sankar *et al.* [8] studied ternary thallium rare-earth chalcogenides *viz.* $TlGdSe_2$, $TlGdTe_2$, and Tl_9GdTe_6. They found that $TlGdSe_2$ and $TlGdTe_2$ crystallize in the α-$NaFeO_2$-type structure and exhibited low thermal conductivity (~0.5 $W \cdot m^{-1} \cdot K^{-1}$) and moderate thermoelectric performance (ZT ~0.5), while Tl_9GdTe_6 showed high electrical conductivity and a low Seebeck coefficient. Duczmal *et al.* [9-12] reported that $TlLnX_2$ (X = S, Se; Ln = rare earths) also adopts the α-$NaFeO_2$-type structure, with magnetic properties attributed to Gd^{3+} ions and ferromagnetically coupled antiparallel layers. Gautam *et al.* [13] found $TlGdSe_2$ to be an indirect bandgap semiconductor (1.36 eV) with a magnetic moment of ~7.0 μB. Yu *et al.* [14] confirmed complex magnetic interactions and indirect bandgaps (~1.26 eV for $TlGdSe_2$ and ~0.26 eV for $TlGdTe_2$) using spin-orbit coupled calculations.

2. Computational method
Density Functional Theory (DFT) [15] has been employed to perform electronic and optical calculations using the full-potential linearized augmented plane wave plus local orbitals (FP-LAPW + lo) method, implemented in the WIEN2K software package [16, 17]. The total density of states in the present study was calculated using

the PBE-GGA exchange-correlation functional [18]. A plane wave cut-off of $R_{MT}Kmax = 6$ was used to ensure convergence, where Kmax represents the plane wave cut-off energy and R_{MT} denotes the muffin-tin radius (the minimum radius of an atomic sphere). For Brillouin zone sampling, the parameters included a cut-off energy of -6.0 Ry, a convergence criterion of 0.001 Ry, and a k-point density of 1000.

The complex dielectric function, $\epsilon(\omega) = \epsilon_1(\omega) + i\epsilon_2(\omega)$, was used to describe the optical properties of these crystalline material. Here, $\epsilon_2(\omega)$ (the imaginary part) represents the material's absorption of electromagnetic radiation at different photon energies, while $\epsilon_1(\omega)$ (the real part) describes the material's polarization response to an external electric field [19-21]. Once $\epsilon_1(\omega)$ and $\epsilon_2(\omega)$ are obtained using the Kramers-Krönig relations and Drude theory [19-21], additional optical parameters such as the refractive index $\eta(\omega)$, extinction coefficient $k(\omega)$, reflectivity $R(\omega)$, optical conductivity $\sigma(\omega)$, absorption coefficient $\alpha(\omega)$, and electron energy-loss function $L(\omega)$ can be derived using following equations [19-21]:

$$\eta(\omega) = [\sqrt{\varepsilon_1^2(\omega) + \varepsilon_2^2(\omega)}\ ] - \varepsilon_1(\omega)]^{1/2}/2^{1/2} \quad \ldots\ldots (1)$$

$$k(\omega) = [\sqrt{\varepsilon_1^2(\omega) + \varepsilon_2^2(\omega)}\ ] - \varepsilon_1(\omega)]^{1/2}/2^{1/2} \quad \ldots\ldots (2)$$

$$\alpha(\omega) = \sqrt{2}\frac{\omega}{c}[\sqrt{\varepsilon_1^2(\omega) + \varepsilon_2^2(\omega)}\ ] - \varepsilon_1(\omega)]^{1/2} \quad \ldots\ldots (3)$$

$$R(\omega) = \frac{(\eta-1)^2+k^2}{(\eta+1)^2+k^2} \quad \ldots\ldots (4)$$

$$L(\omega) = \frac{\varepsilon_2(\omega)}{[\varepsilon|1^2(\omega) + \varepsilon_2^2(\omega)]} \quad \ldots\ldots (5)$$

3. Results and discussion

3.1 Electronic structure: band structure (BS) and density of states (DOS): To analyze the contribution of atomic orbitals to the electronic structure of Tm-based thallium ditelluride, $TlTmTe_2$, spin-polarized electronic band structures were calculated for spin-up and spin-dn using PBE-GGA exchange correlation within DFT along high-symmetry path (Γ-M-K-Γ-A) within the irreducible Brillouin zone. The calculated spin-polarized electronic band structures are illustrated in Figs. 1(a, b). The results reveal a hybrid electronic nature of $TlTmTe_2$ as the spin-up bands show a semiconducting character with a band gap of ~1.87 eV, whereas the spin-down bands confirm metallic character with bands crossing the Fermi level. Such properties make $TlTmTe_2$ a promising candidate for spintronic and magneto-optoelectronic applications.

To examine the contributions of specific atomic orbitals, the total and partial densities of states (TDOS and PDOS) are shown in Fig. 2 and Fig. 3 respectively. The TDOS profiles for both spin channels for the compound $TlTmTe_2$ and its constituent atoms (Tl, Tm, and Te), calculated using the PBE-GGA functional, are presented in Figs. 2 (a-c). A vertical dashed line at 0.00 eV marks the Fermi level. Fig. 2(a) shows that the spin-up channel exhibits a clear gap between the valence and conduction states (~1.83 eV), confirming the semiconducting behavior. In contrast, the spin-down channel shows a finite density of states at the Fermi level, indicating metallic character. This supports the conclusion that $TlTmTe_2$ exhibits 100% spin polarization at the Fermi level, a defining characteristic of half-metals. Fig. 2(b) and 2(c) reveal that in the total density of states (TDOS) of $TlTmTe_2$, the DOS observed around −10.0 eV and −12.0 eV are primarily dominated by Tl-atoms and Te-atoms, respectively. The TDOS near the Fermi level (around 0.0 eV) are predominantly governed by contributions from Tm-atoms, with a minor contribution from Te-atoms.

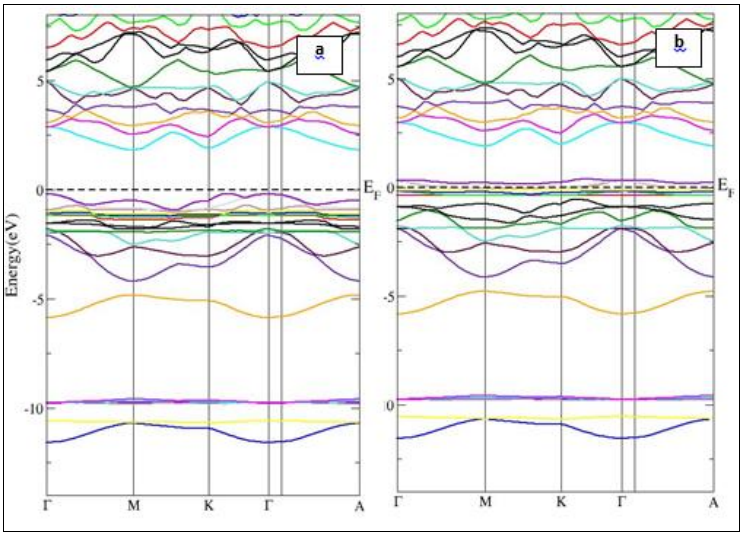

Fig 1: Spin polarized electronic band structure along the high symmetry directions, Γ, M, K and A for (a) $TlTmTe_2$-up (b) $TlTmTe_2$-dn using PBE-GGA.

Further insights are provided by the PDOS plots shown in Figs. 3 (a-f). These figures show that in the total density of states observed around −10.0 eV are mainly dominated by Tl-d orbital electrons and TDOS observed at around −12.0 eV are dominated by Tm-p orbital electrons with small contribution of Te-s orbital electrons. The TDOS positioned near the Fermi level particularly around -1.5 eV for spin-up and at 0.0 eV for spin-down are dominated by Tm-4f orbital electrons which are responsible for magnetic moment and hence magnetic properties in the compound. This confirms the major role of Tm-4f orbitals in the electronic and magnetic properties of the compound. These findings align with the band structure results and affirm $TlTmTe_2$ as a strong candidate for spintronic applications.

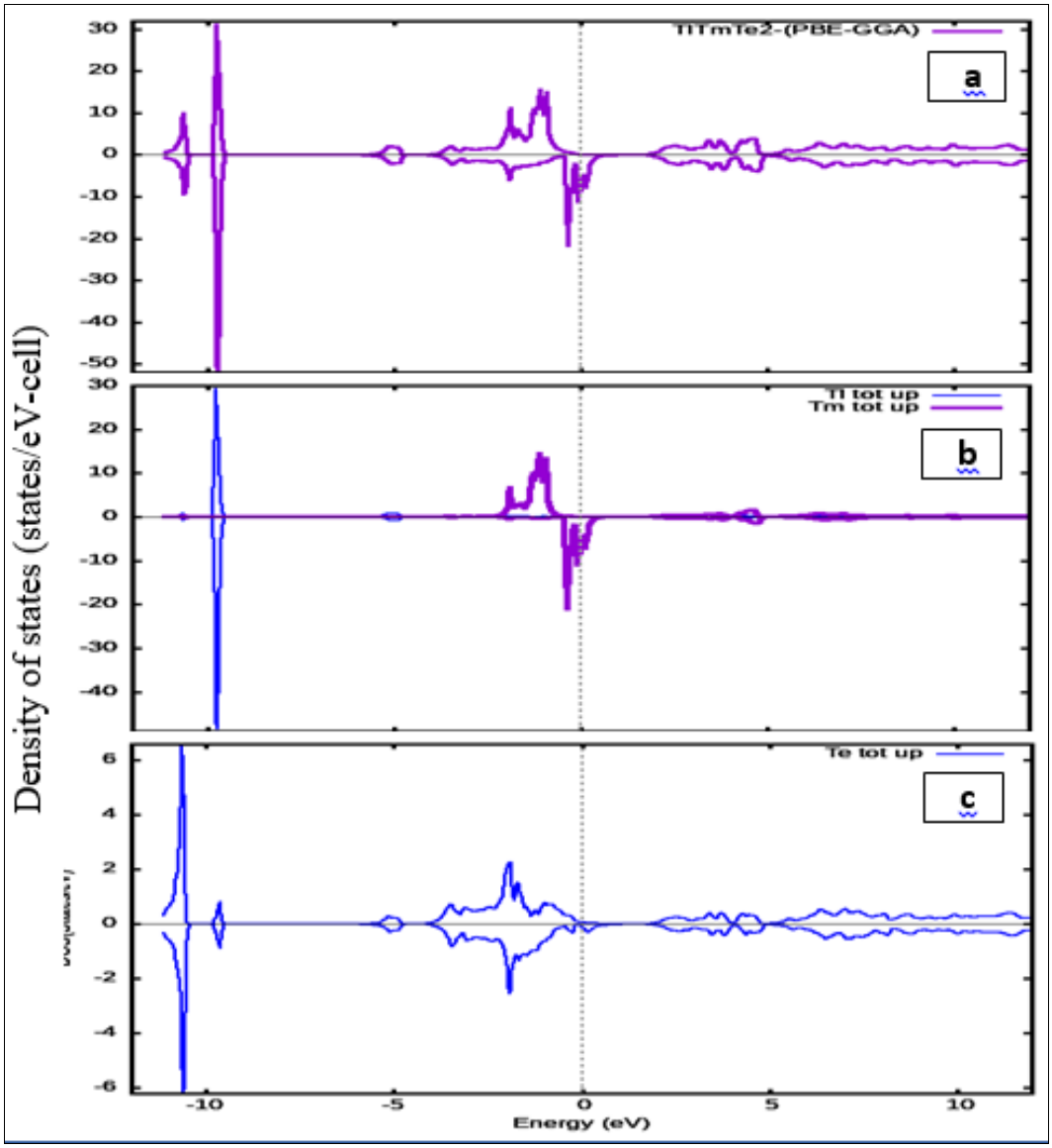

Fig 2: Total density of states for (a) $TlTmTe_2$ (b) Tl and Tm (c) Te using PBE-GGA

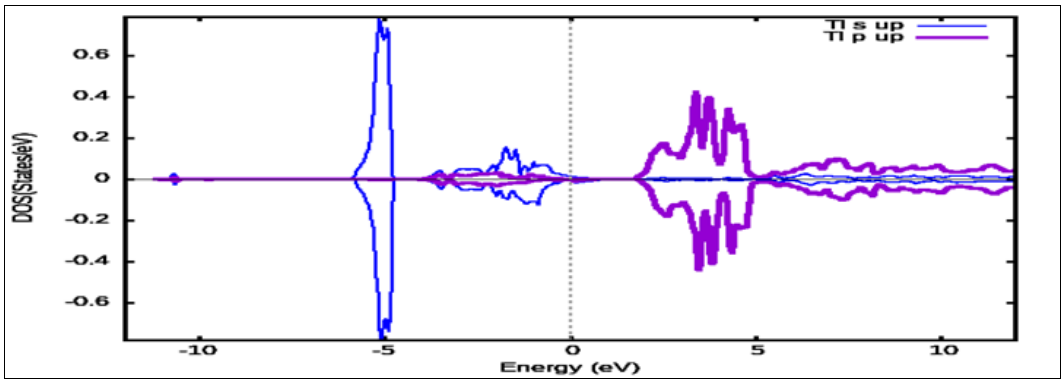

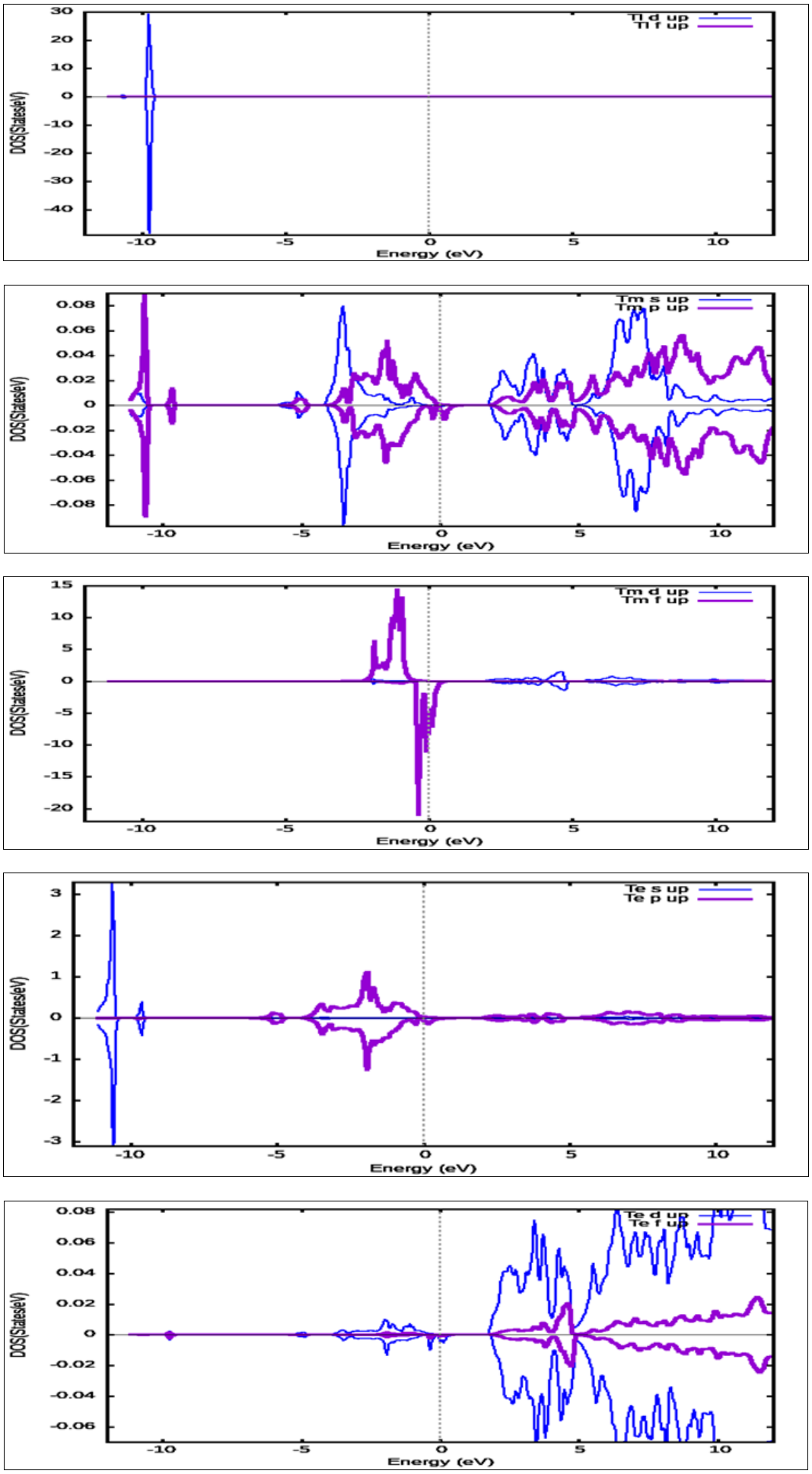

Fig 3: Partial density of states for (a) Tl-s, Tl-p orbitals (b) Tl-d, Tl-f orbitals (c) Tm-s, Tm-p orbitals (d) Tm-d, Tm-f orbitals (e) Te-s, Te-p orbitals (f) Te-d, Te-f orbitals using PBE--GGA.

3.2 Optical Properties

The optical properties of $TlTmTe_2$ play a crucial role in enabling its potential applications in optoelectronics. These properties are closely linked to the electronic structure of a material and its interaction with electromagnetic radiation. The real part of the dielectric function, $\varepsilon_1(\omega)$, characterizes the polarization of material under an electric field, while the imaginary part, $\varepsilon_2(\omega)$, represents optical absorption. The energy-dependent variation of $\varepsilon_1(\omega)$ is shown in Fig. 4(a). The static dielectric constant $\varepsilon_1(0)$ estimated to be ~ 27.0 along the x-axis and 15.0 along z-directions, suggesting larger anisotropy in the IR region and significant electronic polarization. A peak at ~3.0 eV corresponds to interband transitions primarily involving Tm-4f orbital excitations in the UV range. $\varepsilon_1(\omega)$ becomes negative beyond ~ 4.0 eV along z-axis and ~5.0 eV along x-axis and reaching at minimum value at ~ 6.0 eV, indicating metallic reflectivity and optical opacity at these energies. Fig. 4 (b) exhibit the variation of $\varepsilon_2(\omega)$ with photon energy. It shows a strong absorption peak around 4.0 eV for both the axis, confirming significant electronic transitions between valence and conduction bands. The first critical point, or absorption onset, appears near to ~ 0.0 eV, consistent with the half-metallic nature of $TlTmTe_2$.

Fig. 4 (c) depicts the variation of refractive index, $\eta(\omega)$ with photon energy which is important parameter for optical design. It shows that static refractive index, $\eta(0)$ is ~ 5.20 along x-axis and 3.9 along z-axis, consistent with the Penn model [22]. A strong peak at ~3.0 eV indicates anomalous dispersion, transitioning to normal dispersion at higher energies

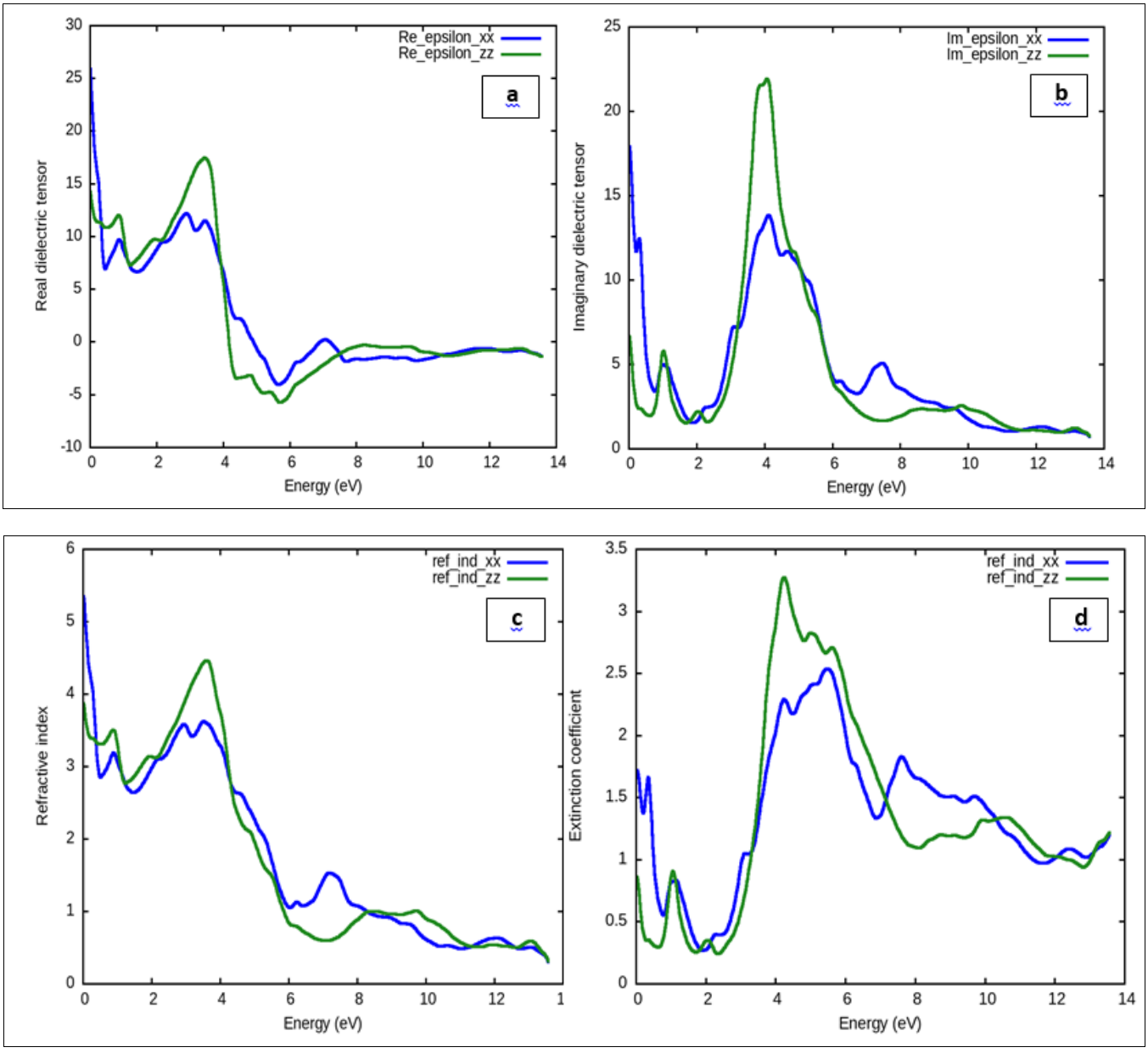

Fig 4: Variation of (a) Real part of dielectric function, $\varepsilon_1(\omega)$ (b) Imaginary part of dielectric function, $\varepsilon_2(\omega)$(c) refractive index, $\eta(\omega)$ (d) Extinction coefficient, $k(\omega)$ along x- and z- axis with photon energy using PBE-GGA.

The extinction coefficient $k(\omega)$, which measures light attenuation, is derived from $\varepsilon_1(\omega)$ and $\varepsilon_2(\omega)$ as follows [23]:

$\eta^2 - k^2 = \varepsilon_1(\omega)$ and $2\eta k = \varepsilon_2(\omega)$……(6)

The variation of k(ω) with photon energy is shown in Fig. 4(d). As shown in Fig. 4(d), higher k(ω) values along the z-direction in the UV range indicate strong directional absorption, reinforcing the material's suitability for UV-based optoelectronic applications.

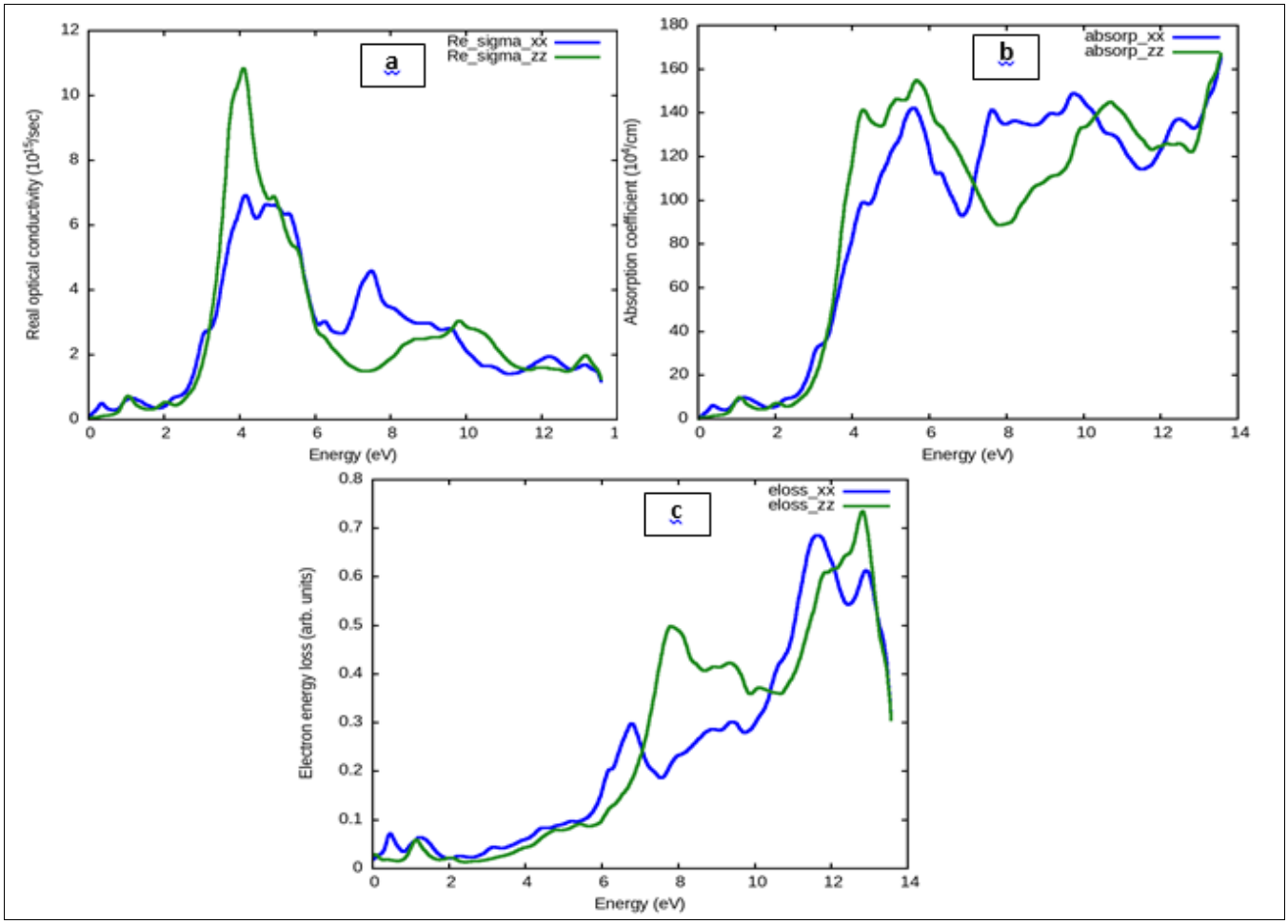

Fig 5: Variation of (a) optical conductivity, σ(ω) (b) absorption coefficient, α(ω) (c) Electron energy loss, L (ω) along x- and z- axis with photon energy using PBE-GGA.

The optical conductivity σ(ω) is calculated by $\sigma(\omega) = -(\frac{i\omega}{4\pi})$ $\varepsilon_2(\omega)$ [22] is presented in Fig. 5 (a). Fig. 5 (a) shows that σ(ω) rises sharply from 0.0 eV and get high peaks between ~4.0-6.0 eV in the UV range. This reflects strong optical transitions and confirms the material's metallic nature in this energy window. Beyond 6.0 eV, σ(ω) decreases due to fewer available electronic states and reduced transition probabilities. The absorption coefficient α(ω) is shown in Fig. 5 (b). It exhibits low values in the IR region but increases sharply in the UV region (~4.0-7.0 eV), confirming high UV absorption which is a desirable characteristic for UV filters, photodetectors, and solar absorber devices.

Lastly, the energy loss function L(ω), plotted in Fig. 5(c), captures plasmonic behavior, with significant peaks at ~8.0 eV and 12.0 eV along z-axis and ~7.0 eV and 11.5 eV along x-axis, corresponding to the plasma frequency (ω_{pl}) of $TlTmTe_2$. These peaks mark the energy ranges where the material experiences maximum energy loss due to collective oscillations of free electrons, essential for understanding energy dissipation mechanisms in optical systems.

4. Conclusions

The optical and electronic behavior of $TlTmTe_2$ was investigated in the present study using DFT calculations with PBE-GGA correlation functional. Electronic structure analysis revealed that $TlTmTe_2$ exhibit half-metallic character, with a dominance of spin-down states at the Fermi level. The optical characteristics indicate larger anisotropy in the infrared (IR) region and slight anisotropy beyond the IR region. The optical threshold energy was found to be approximately 0.0 eV, consistent with the half-metallic nature of the compound. The estimated static real dielectric constant, $\varepsilon_1(0)$ and static refractive index, η(0) was found align well with the predictions of the Penn Model, supporting the reliability of the optical calculations. The optical conductivity, σ(ω) spectra show a rise starting from 0.0 eV confirms the metallic nature of $TlTmTe_2$. The observed decrement in σ(ω) beyond 4.0 eV can be attributed to: (i) a reduction in the available states for electronic transitions at higher energies, (ii) the absence of high-energy excitations, and (iii) a decrease in the density of states at elevated energy levels.

Furthermore, the strong absorption in the ultraviolet (UV) region (> 4.0 eV) indicates maximal attenuation due to photon absorption, making these materials promising candidates for UV-absorber systems such as photovoltaics, where efficient sunlight absorption is essential for generating electrical energy.

References

1. Fomina KA, Marchenkov VV, Shreder EI, Weber HW. Electrical and optical properties of X_2YZ (X = Co, Fe; Y

= Cr, Mn, Ti; Z = Ga, Al, Si) Heusler alloys. Solid State Phenom. 2011;168:545-548.
2. Yang LH. Half-metallic materials and their properties. London: Imperial College Press; 2013. ISBN: 978-1-908977-12-0.
3. Prinz GA. Spontaneous spin polarization of electrons by diluted magnetic heterostructures. Phys Today. 1995;48:58.
4. Wolf SA, Awschalom DD, Buhrman RA, Daughton JM, von Molnar S, Roukes ML. Spintronics: a spin-based electronics vision for the future. Science. 2001;294:1488.
5. Şaşıoğlu E, Sandratskii LM, Bruno P, Galanakis I. Exchange interactions and temperature dependence of magnetization in half-metallic Heusler alloys. Phys Rev B. 2005;72:184415.
6. Antonov V, Harmon B, Yaresko A. Electronic structure and magneto-optical properties of solids. New York: Kluwer Academic Publishers; 2004.
7. Everhart W, Newkirk J. Mechanical properties of Heusler alloys. Heliyon. 2019;5(5):e01578.
8. Sankar R, Sanasy SB, Kleinke H. J Electron Mater. 2012;41(6):1662-1666.
9. Duczmal M, Pawlak L. J Alloys Compd. 1994;209:271-4.
10. Duczmal M, Pawlak L. J Alloys Compd. 1995;219:189-92.
11. Duczmal M, Pawlak L. J Alloys Compd. 1997;262-3:316.
12. Duczmal M, Pawlak L, Pokrzywnicki S. Acta Phys Pol A. 2000;97:839.
13. Gautam R, Kumar A, Singh RP. Acta Phys Pol A. 2017;132(4).
14. Vyazovskaya AY, Petrov EK, Koroteev YM, Bosnar M, Silkin IV, Chulkov EV, *et al.* Superlattices of gadolinium and bismuth-based thallium dichalcogenides as potential magnetic topological insulators. Nanomaterials (Basel). 2023;13(1):38. doi:10.3390/nano13010038.
15. Blom A. Density functional theory for beginners. Lund: Lund University; 2002.
16. Ota Y, Imura M, Banal RG, Koide Y. J Phys D Appl Phys. 2022;55:455102.
17. Blaha P, Schwarz K, Tran F, Laskowski R, Madsen GKH, Marks LD. J Chem Phys. 2020;152:074101.
18. Blaha P, Schwarz K, Tran F, Laskowski R, Madsen GKH, Marks LD. J Chem Phys. 2020;152(7):074101.
19. Ehrenreich H, Cohen MH. Self-consistent field approach to the many-electron problem. Phys Rev. 1959;115:786.
20. Marius G. The physics of semiconductors: Kramers-Kronig relations. Berlin Heidelberg: Springer; 2010. p. 775-6.
21. Hadjab M, Ibrir M, Berrah S, Abid H, Saeed MA. Optik. 2018;169:69-76.
22. Penn D. Phys Rev. 1962;128:2093.
23. Wooten F. Optical properties of solids. New York: Academic Press; 1972.